

Interpretation of the cross-correlation function of ACE and STEREO solar wind velocities using a global MHD Model

Pete Riley,¹ J. Luhmann,² A. Opitz,³ J. A. Linker,¹ and Z. Mikic¹

Received 25 May 2010; revised 7 July 2010; accepted 13 August 2010; published 13 November 2010.

[1] Measurements from the ACE and STEREO A and B spacecraft are allowing an unprecedented view of the structure of the three-dimensional heliosphere. One aspect of this is the degree to which the measurements at one spacecraft correlate with those at the other. We have computed the cross-correlation functions (CCFs) for all three combinations of ACE and STEREO A and B in situ observations of the bulk solar wind velocity as the spacecraft moved progressively farther away from one another. Our results confirm previous studies that the phase lag between the signals becomes linearly larger with time. However, we have identified two intervals where this appears to break down. During these “lulls,” the CCF reveals a phase lag considerably less than that which would be predicted based only on the angular separation of the spacecraft. We modeled the entire STEREO time period using a global MHD model to investigate the cause for these “lulls.” We find that a combination of time-dependent evolution of the streams as well as spatial inhomogeneities, due to the latitudinal separation of the spacecraft, are sufficient to explain them.

Citation: Riley, P., J. Luhmann, A. Opitz, J. A. Linker, and Z. Mikic (2010), Interpretation of the cross-correlation function of ACE and STEREO solar wind velocities using a global MHD Model, *J. Geophys. Res.*, 115, A11104, doi:10.1029/2010JA015717.

1. Introduction

[2] The STEREO (Solar Terrestrial Relations Observatory) spacecraft launched on 25 October 2006 on a Delta II rocket. Since early 2007, it has been continuously returning a wide range of remote solar and in situ measurements of the Sun’s corona and the inner heliosphere. Charged with a number of fundamental scientific objectives, one of particular relevance to this study is to improve our understanding of the structure of the ambient solar wind. With nearly identical instrumentation, the STEREO ahead (A) and behind (B) spacecraft are separating by $\sim 45^\circ$ per year. Restricted to the ecliptic plane, in addition to the monotonically increasing longitudinal separation, the spacecraft also separate from one another in radial separation (up to a maximum of ~ 0.15 AU) as well as in heliographic latitude (up to a maximum separation of $\sim 14.4^\circ$). The ACE (Advanced Composition Explorer) spacecraft launched on 25 August 1997, and since then has provided a continuous stream of in situ measurements of the solar wind [Stone *et al.*, 1998]. The measurements from STEREO A and B, coupled with those from ACE, thus represent a unique data set from which to study the effects of spatial and temporal evolution of solar wind streams, and, in particular, to assess the degree of correlation between them.

[3] Previous studies have investigated the correlation of solar wind stream structure from one and multiple spacecraft. The first comprehensive auto-correlation analysis of in situ solar wind data was performed by Gosling and Bame [1972]. Using solar wind speed data from the Vela 2 and 3 missions, they assessed to what extent solar wind structure persisted from one rotation to the next. They found that the average correlation was only 0.3, suggesting that most structure did not persist from one rotation to the next; However, this coefficient varied from 0.1 to 0.7 at different times. They also noted that differential rotation affected the results, the implication being that a wide range of heliolatitudes contributed to the solar wind measured at Earth. In a more comprehensive analysis, Gosling *et al.* [1976] found that the most stable stream structure occurred during the declining phase of the solar cycle. Richardson *et al.* [1998] cross-correlated data from ISEE 3 at L1 and IMP 8 at Earth for times corresponding to near-solar maximum conditions. They found that the temporal lag between the structures observed at the two spacecraft depended on both the radial and azimuthal separation. Additionally, they found that the lag required a correction due to corotation, that is, that the stream normals are tilted away from the radial direction and toward the direction of planetary motion. In contrast, Paularena *et al.* [1998], investigating the correlation between data observed by IMP 8, Interball-1, and Wind during near-solar minimum conditions, found that the correlation depended only on the radial separation of the spacecraft and not on the azimuthal separation. Moreover, they did not find any need to correct for corotation. Richardson *et al.* [1998] suggested that the smaller angular separation of the spacecraft in the Paularena *et al.* [1998]

¹Predictive Science, San Diego, California, USA.

²SSL, University of California, Berkeley, California, USA.

³Centre d’Etude Spatiale des Rayonnements (CNRS-UPS), University of Toulouse, Toulouse, France.

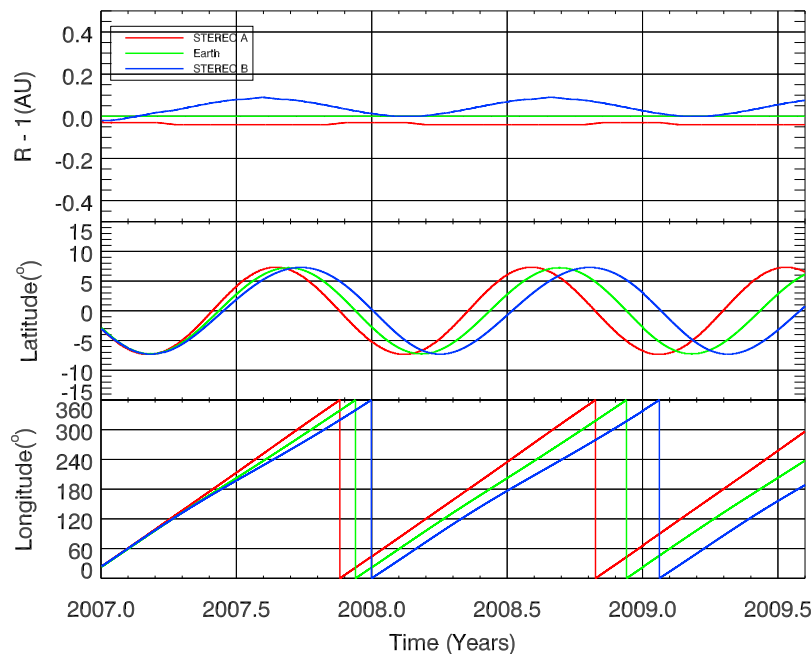


Figure 1. Ephemeris data for the ACE and STEREO spacecraft. In each frame, the red curve corresponds to the location of STEREO A, the blue curve to the location of STEREO B, and the green curve to the location of ACE. (top) The heliocentric location of the spacecraft, plotted relative to 1 AU. (middle) The heliographic latitude of the spacecraft. (bottom) The heliographic, inertial longitude of the spacecraft.

study, together with the fact that the two investigations used data from different extremes of the solar cycle could account for these apparent contradictions.

[4] *Podesta et al.* [2008] first reported on the correlation length of large-scale solar wind velocity fluctuations measured at STEREO A and B. They focused on the interval between February 2007 and August 2007, corresponding to near-solar minimum conditions. They found that the transverse correlation length was 0.25 ± 0.02 AU. *Opitz et al.* [2009] analyzed the solar wind velocity from STEREO A and B from March to August of 2007. Their study focused on the temporal evolution of the solar wind at the two spacecraft by removing spatial effects caused by the radial and angular separation of the two spacecraft. In particular, they time-shifted STEREO B, accounting for both longitudinal and radial separation and computed the correlation coefficient between it and STEREO A data. They found that the correlation decreased with increasing separation (and time). However, they noted some exceptions to the otherwise good correlations found: (1) day 142, 2007, which coincided with an ICME; (2) day 155, 2007, associated with a CIR; (3) day 201, 2007, which coincided with significant velocity gradient bisecting the $\sim 2^\circ$ latitudinal separation of the spacecraft [*Rouillard et al.*, 2009]; and (4) days 227–235, 2007. They ascribed the poor correlation during the first portion of this last interval (days 227–231) to temporal evolution of the solar wind source as it moved from under one spacecraft to the other. Since the stream structure of the second half of this interval remained intact one rotation later, they suggested that the poor correlation was due to spatial inhomogeneities.

2. Orbits of the ACE and STEREO Spacecraft

[5] The relative locations of the ACE and STEREO spacecraft obviously play an important role in understanding

the large-scale correlation of solar wind parameters. Figure 1 summarizes the heliocentric distance, latitude, and longitude of the spacecraft, together with the differences between them. In Figure 1 (top), $R - 1$ is plotted, showing that the STEREO spacecraft oscillate about values slightly less or more than 1 AU. These oscillations are synchronous so that during mid/late 2007, 2008, and 2009 the spacecraft have a maximum radial separation of ~ 0.13 AU. We can estimate the maximum temporal lag between the STEREO spacecraft due to the radial separation using $\Delta t = \Delta r / v_{sw}$. Assuming $v_{sw} = 600$ km s^{-1} , we obtain $\Delta t \sim 9$ h. The temporal lag due to longitudinal effects obviously begins to dominate once the spacecraft are separated by $\sim \frac{1 \text{ day}}{27 \text{ days}} \times 360^\circ \sim 13^\circ$. Following launch, the two STEREO spacecraft maintained their position in the ecliptic plane, but as they moved farther away from Earth (and hence ACE), their heliographic latitudinal separation began to oscillate, the amplitude of which became progressively larger. Maximum latitudinal differences occurred at the shortly before the beginning of, and midway through each year. Finally, in Figure 1 (bottom), the inertial longitude of the three spacecraft is shown. Of particular note is that this separation is not strictly linear: Prior to, and during the early portion of each calendar year, the increase in separation is modest, whereas, for the remainder of the year, it is more pronounced.

[6] In this study, we investigate the evolving cross-correlation functions (CCFs) computed from 1 h averaged solar wind velocity measurements from the PLASTIC instruments [*Galvin et al.*, 2008] onboard STEREO A and B and the SWEPAM instrument onboard ACE [*McComas et al.*, 1998]. The three spacecraft allow us to compute three CCFs: (1) STEREO B/ACE; (2) ACE/STEREO A; and (3) STEREO B/ACE. Unlike the previous study of *Opitz et al.* [2009], which did not include near-Earth measurements, we do not assume and apply a phase lag between the measurements

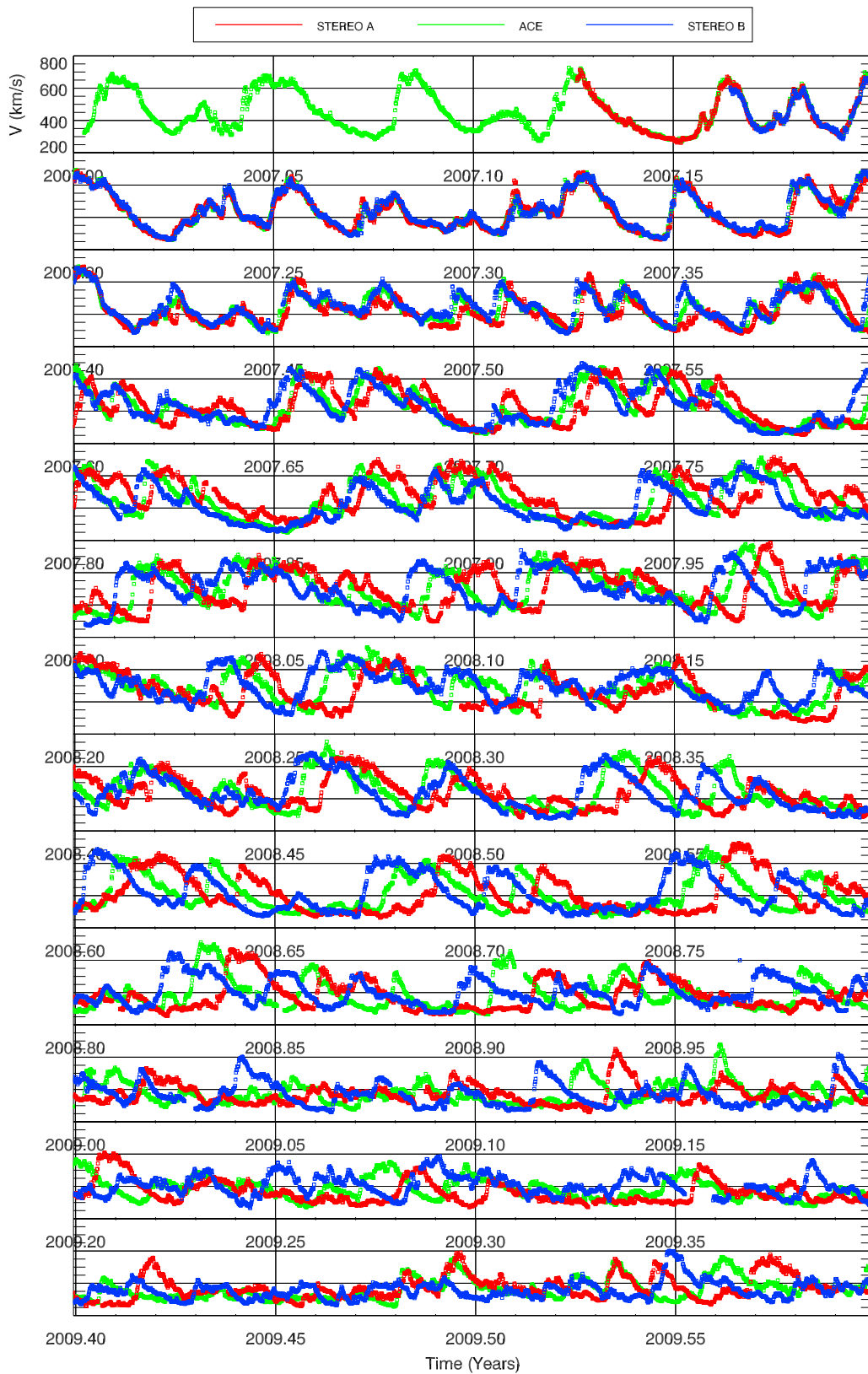


Figure 2. Bulk solar wind speed from (top) 2007.0 through (bottom) 2009.5. Green, red, and blue correspond to ACE, STEREO A, and STEREO B, respectively. A movie illustrating the evolution of these streams can be viewed/downloaded at <http://www.predsci.com/stereo/movies/>.

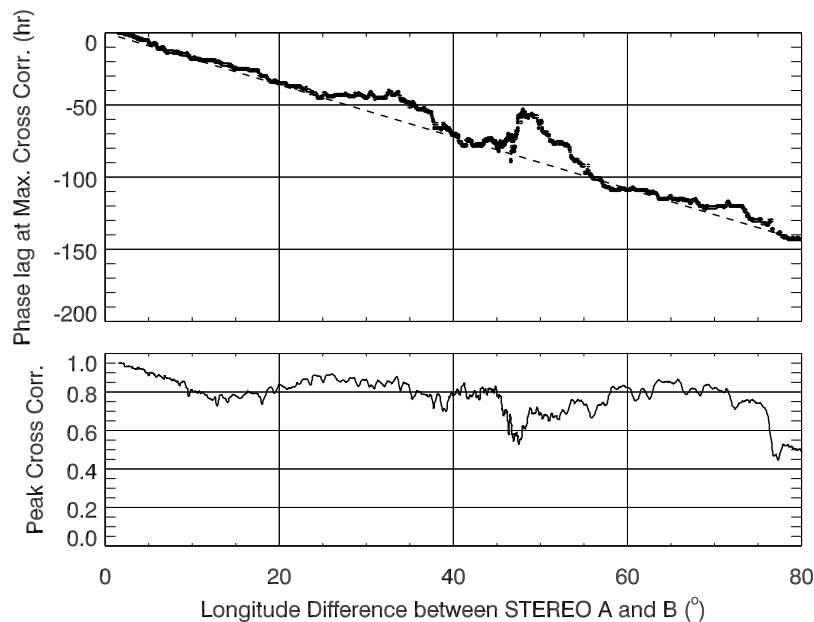


Figure 3. (top) The temporal phase lag that maximizes the cross-correlation function (CCF) between the solar wind velocities measured at STEREO B and A, plotted as a function of longitudinal separation of the spacecraft. (bottom) The correlation coefficient corresponding to the phase lag in the plot above.

from which a correlation coefficient is computed, but rather compute the temporal phase lag between each pair of spacecraft that maximizes the CCF. To a first approximation, the results match our intuition and previous studies, that the phase lag increases linearly with the angular separation of the spacecraft; However, there are two interesting intervals, in particular, where the phase lag “pauses.” We use global MHD model solutions to show that these intervals are due to a combination of both temporal and spatial effects.

3. Analysis of ACE and STEREO In Situ Bulk Solar Wind Speed Observations

[7] In general, the CCF between two continuous functions is the integral of the complex conjugate of one variable and the time-shifted value of the other variable,

$$(f \hat{a} g)(\Delta t) = \int_{-\infty}^{\infty} f^*(\tau)g(\Delta t + \tau)d\tau. \quad (1)$$

Extending this to real-valued discrete functions of finite length, which in this study are the bulk solar wind velocities measured at the two spacecraft (v_A and v_B) over some temporal lag, Δt , we can define the CCF to be

$$\begin{aligned} (v_A \hat{a} v_B)(\Delta t) &= \frac{\sum_{k=0}^{N-|\Delta t|-1} (v_{A,k+|\Delta t|} - \bar{v}_A)(v_{B,k} - \bar{v}_B)}{\sqrt{\left[\sum_{k=0}^{N-1} (v_{A,k} - \bar{v}_A)^2\right] \left[\sum_{k=0}^{N-1} (v_{B,k} - \bar{v}_B)^2\right]}} \text{for } L < 0 \\ &= \frac{\sum_{k=0}^{N-|\Delta t|-1} (v_{A,k} - \bar{v}_A)(v_{B,k+\Delta t} - \bar{v}_B)}{\sqrt{\left[\sum_{k=0}^{N-1} (v_{A,k} - \bar{v}_A)^2\right] \left[\sum_{k=0}^{N-1} (v_{B,k} - \bar{v}_B)^2\right]}} \text{for } L > 0, \end{aligned} \quad (2)$$

where \bar{v}_A and \bar{v}_B are the mean values of variables between 0 and $N - 1$ (The algorithm used to compute this function is

available as part of the Interactive Data Language (IDL) numerical package (`c_correlate.pro` in the main library directory)).

[8] Thus, for two real-valued functions (v_A and v_B), which differ only by a shift along the time axis, we can compute the CCF for a range of time lags (Δt). Where the functions match, the peaks and troughs become aligned, making a positive contribution to the summation, and the CCF is maximized. In the specific case of bulk solar wind velocities, which are always positive, the CCF maximum is weighted more by the fast solar wind streams, than the slow wind, since they contribute proportionately more to the summations.

[9] Figure 2 illustrates graphically how the time shift that maximizes the CCF increases as the angular separation of the spacecraft becomes larger. We can estimate how we would expect the time lag (Δt) that maximizes the CCF to increase with angular separation ($\Delta \lambda$). It is simply the fraction of a solar rotation by which the spacecraft are separated. Thus, we anticipate that the phase lag should change by

$$\Delta t = -\frac{\tau_{rot}}{360^\circ} \Delta \lambda, \quad (3)$$

where τ_{rot} is the rotation period of the Sun, and we have chosen a negative decrease to reflect a convention that it is the amount of time that measurements from the ahead spacecraft must be shifted back in time to align with the spacecraft located at an earlier longitude. As a concrete example, at a separation of 55.5° , the predicted absolute phase lag would be ~ 100 h, or a little over 4 days. It is worth noting that the synodic ($\tau_{rot} = 27.27$ days), rather than the sidereal ($\tau_{rot} = 25.38$ days) period is the appropriate interval to use, since the spacecraft are drifting in an Earth-based reference frame, and not some fixed inertial point in space.

[10] In Figure 3 (top), we have identified and plotted the phase lag of the peak of the computed CCF as a function of

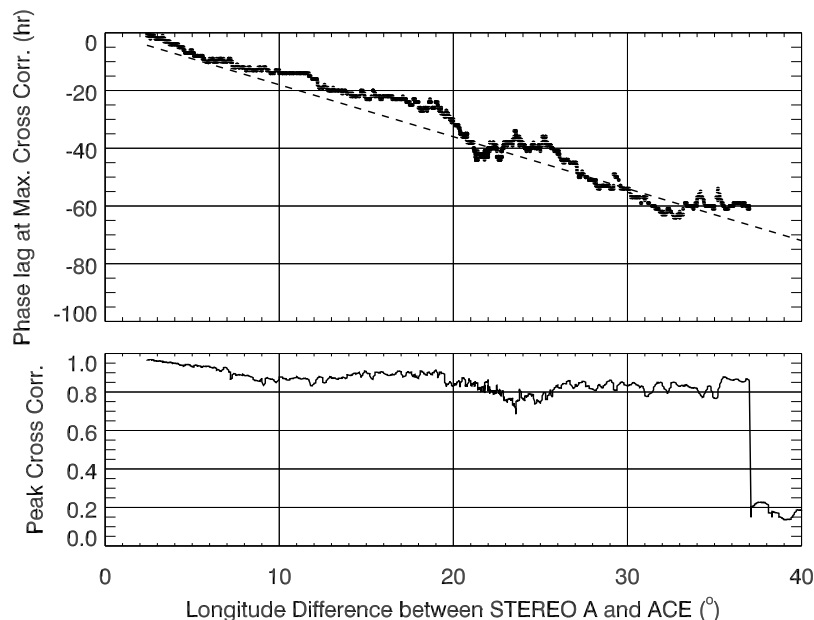


Figure 4. As in Figure 3, but for ACE and STEREO A. Note that the scales for the (top and bottom) abscissa and (top) ordinate span half the range of those in Figure 3.

the STEREO A and B spacecraft separation. A CCF was computed every 10^{-3} years and each CCF was computed using a window of 0.1 years. The phase lag was identified automatically by locating the peak in the CCF and all CCFs were visually inspected to verify that the peak represented a pronounced maximum in the distribution. The anticipated phase lag from equation (3) is shown by the dashed line. To a first approximation, then the computed phase lag matches the simple formula. That is, the phase lag increases linearly with time. However, two obvious deviations are apparent. Since they represent intervals where the phase lag appears to

“pause” from its trend of increasing, we refer to them as “lulls.” The first is centered on Carrington rotation (CR) 2061 (which spanned from 10 September 2007 to 8 October 2007, or days 253 through 281), while the second is centered on CR 2069 (which spanned from 16 April 2008 to 13 May 2008, or days 107 through 134). Both intervals encompass approximately the same duration in longitude, $\sim 12.5^\circ$, corresponding to ~ 3.5 months or 101 days. Whereas the first has the appearance of a “pause,” in the sense that the phase lag holds steady at -45 h before returning to its expected value, the second shows a significant reversal in the trend of increasing lag: Where the

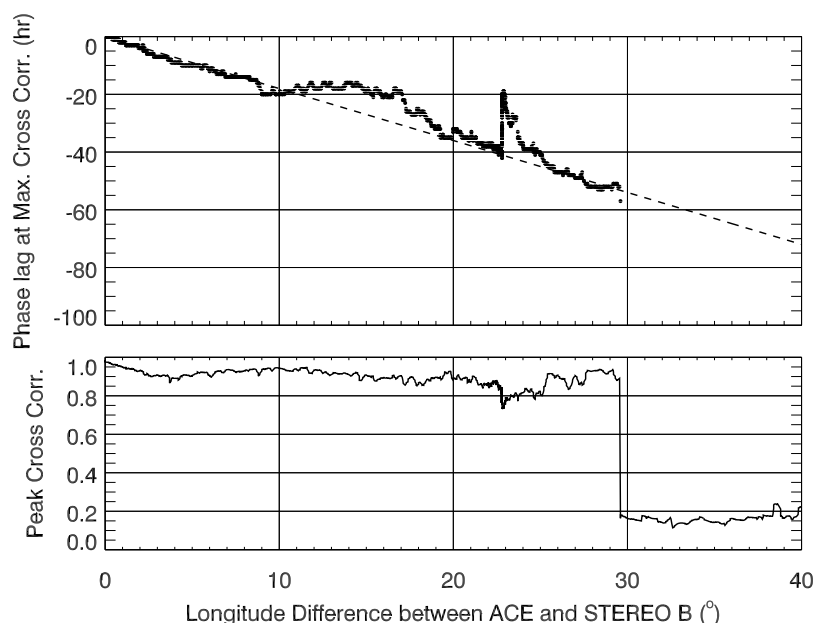


Figure 5. As in Figure 3, but for STEREO B and ACE.

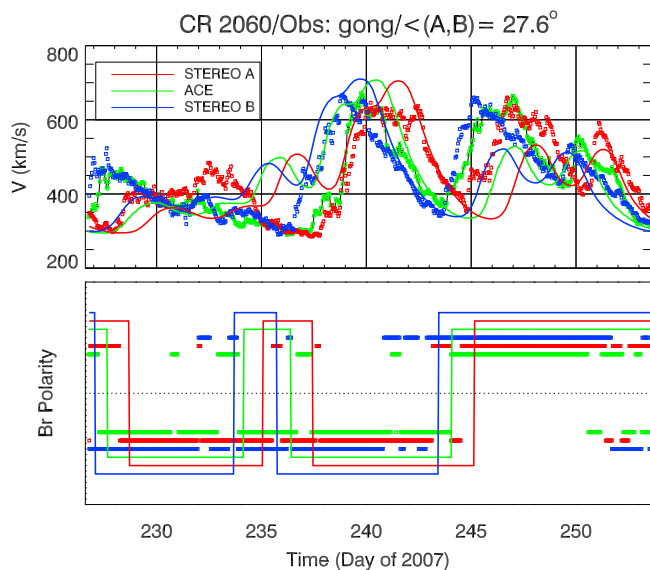


Figure 6. Comparison of model results with (top) in situ speed and (bottom) radial IMF polarity for Carrington rotation (CR) 2060. The solid lines are model results, and the symbols are in situ measurements from ACE (green), STEREO A (red), and STEREO B (blue). The amplitude of polarities have been adjusted to more easily show the variations at each spacecraft; there is no physical significance however to them.

predicted lag would have been -90 h, the computed lag was only -55 h, a difference of 35 h, or 19.4° in effective longitude.

[11] In Figure 3 (bottom), we show the value of the peak correlation coefficient at that phase lag. Thus, until the STEREO spacecraft reached a separation of $\sim 75^\circ$, the correlation coefficient exceeded 0.6 and, for the majority of the time remained near 0.8 . We note that during the first lull, the peak cross-correlation coefficient was slightly higher than the surrounding values, but during the second lull, it was markedly lower. Beyond $\sim 75^\circ$, as the peak correlation coefficient decreased, multiple peaks appeared, and, while it would have been possible to force a local phase lag that matched our expectations based on equation (3), the low value of the correlation coefficient would cast doubt on any inferences drawn.

[12] We performed a similar analysis for ACE and STEREO A. The results are shown in Figure 4. We have scaled the plot to half the maximum values of Figure 3 so that features can be compared directly. In particular, by scaling the longitude to half the maximum value of Figure 3, the two panels span the same duration in time. In the top, we can see similar lulls centered at approximately 17° and 29° . These are roughly half the longitudinal separations for the lulls found in the analysis of STEREO A/B, and thus occur at the same time. Concerning the duration of the lulls; while the second one lasts approximately the same duration in time, the first appears to be significantly broader. We also note that the peak cross-correlation coefficient is, on average slightly larger for this pair of spacecraft; a predictable result given that the spacecraft are closer to one another.

[13] Finally, in Figure 5, we summarize the cross-correlation analysis for STEREO B and ACE. Here the first lull is approximately the same duration as in Figure 3, while the

second one is slightly shorter. More strikingly, the second lull shows a steep initial rise from -40 h to less than -20 h, with a subsequent slower decay back to the predicted phase lag.

4. Global MHD Model Solutions for the STEREO Era

[14] The first MHD models of the solar corona were developed almost 40 years ago [Endler, 1971; Pneuman and Kopp, 1971]. Over the years they have become progressively more sophisticated [Steinolfson et al., 1982; Linker et al., 1990; Mikić and Linker, 1994], culminating in models that include the photospheric field as a boundary condition [Usmanov, 1993; Mikić et al., 1996; Riley et al., 2001a; Roussev et al., 2003]. Complementary efforts focusing on heliospheric models, where the inner boundary was placed beyond the outermost critical point, have also been pursued [Dryer et al., 1978; Pizzo, 1978; Smith and Dryer, 1990; Detman et al., 1991; Odstrčil, 1994]. Most recently, coronal

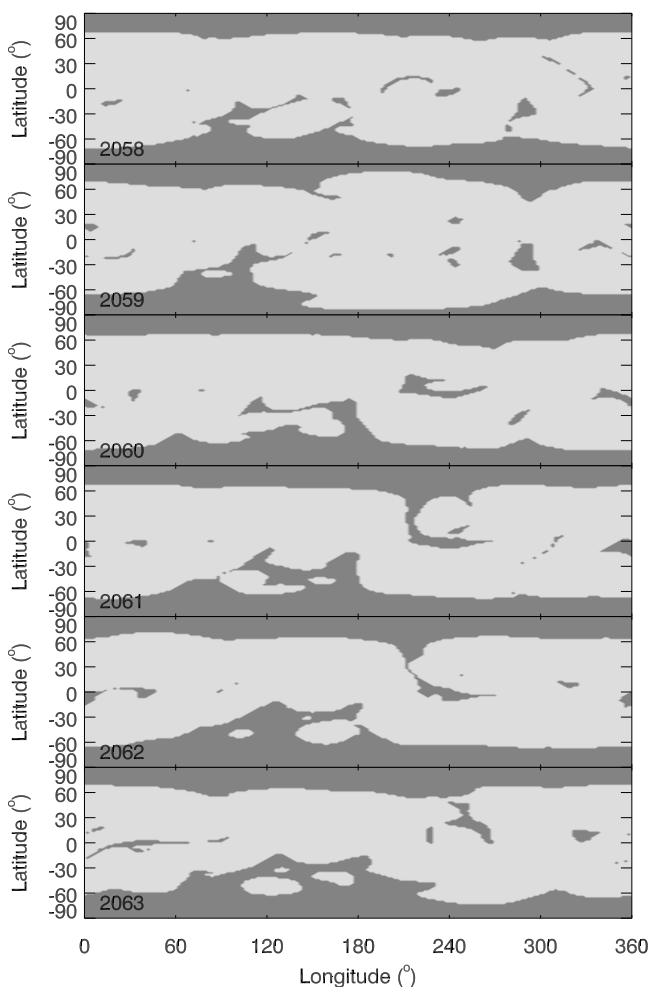


Figure 7. The computed coronal holes for CRs 2058 through 2063. These were obtained by tracing magnetic field lines outward from the photosphere and into the heliosphere. If the field line returned to the photosphere, it was labeled “closed” and shaded light gray, whereas if it reached the outer radial boundary of the simulation domain, it was labeled “open” and shaded dark gray.

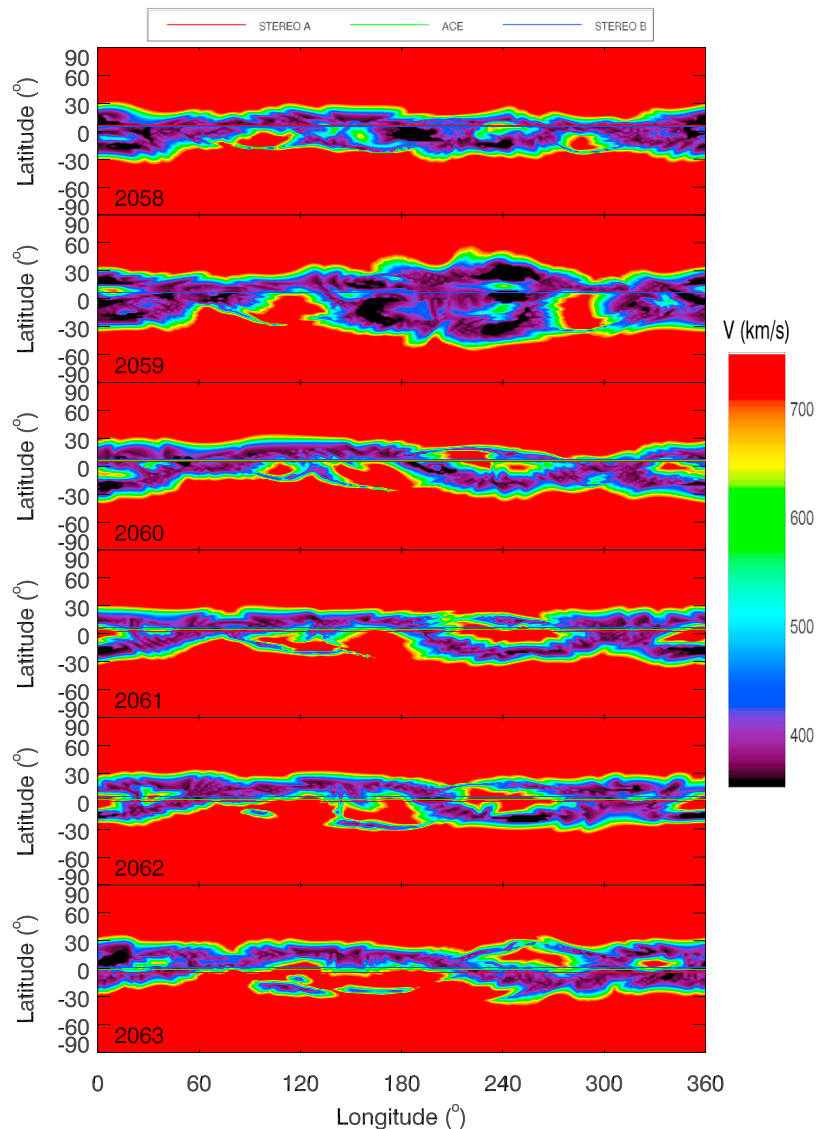


Figure 8. The computed radial solar wind velocities for CRs 2058 through 2063. These were obtained by mapping a photospheric velocity profile [see *Riley et al.*, 2001a] outward along open field lines to $30 R_S$. Red corresponds to $\sim 750 \text{ km s}^{-1}$, while black corresponds to $\sim 350 \text{ km s}^{-1}$.

and heliospheric models have been coupled [*Riley et al.*, 2001a, 2002; *Odstrcil et al.*, 2002; *Riley et al.*, 2003; *Odstrcil et al.*, 2004; *Manchester et al.*, 2006; *Riley et al.*, 2007] and more sophisticated descriptions of energy transport processes have been included [*Lionello et al.*, 2001, 2009].

[15] We have computed global coronal and heliospheric polytropic MHD solutions spanning more than 35 years, and, in particular, for the entire STEREO mission to date (available at <http://www.predsai.com/stereo/>). An important feature that makes our approach unique is the use of observed photospheric magnetograms to drive the solutions. Studies comparing model results with eclipses [*Mikic et al.*, 2002; *Mikić et al.*, 2007] as well as in situ observations at Ulysses and near Earth have shown that we can reproduce the basic features of the solar corona and inner heliosphere [*Riley et al.*, 1996, 2001a, 2001b, 2002, 2003; *Riley*, 2007].

[16] In general, our three-dimensional, time-dependent algorithm solves the following form of the resistive MHD equations on a nonuniform grid in spherical coordinates:

$$\nabla \times \mathbf{B} = \frac{4\pi}{c} \mathbf{J}, \quad (4)$$

$$\nabla \times \mathbf{E} = -\frac{1}{c} \frac{\partial \mathbf{B}}{\partial t}, \quad (5)$$

$$\mathbf{E} + \frac{\mathbf{v} \times \mathbf{B}}{c} = \eta \mathbf{J}, \quad (6)$$

$$\frac{\partial \rho}{\partial t} + \nabla \cdot (\rho \mathbf{v}) = 0, \quad (7)$$

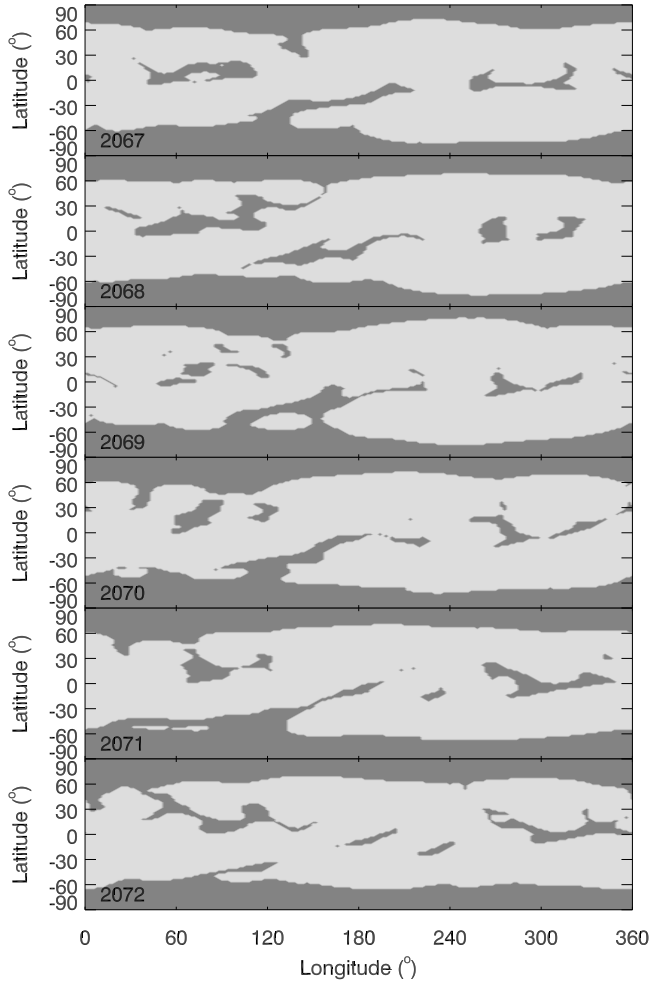


Figure 9. As in Figure 7, but for CRs 2067 through 2072.

$$\frac{1}{\gamma - 1} \left(\frac{\partial T}{\partial t} + \mathbf{v} \cdot \nabla T \right) = -T \nabla \cdot \mathbf{v} + \frac{m_p}{2k\rho} S, \quad (8)$$

$$\rho \left(\frac{\partial \mathbf{v}}{\partial t} + \mathbf{v} \cdot \nabla \mathbf{v} \right) = \frac{1}{c} \mathbf{J} \times \mathbf{B} - \nabla(p + p_w) + \rho \mathbf{g} + \nabla \cdot (\nu \rho \nabla \mathbf{v}), \quad (9)$$

$$S = (-\nabla \cdot \mathbf{q} - n_e n_p Q(T) + H_{\text{ch}}) \quad (10)$$

where \mathbf{B} is the magnetic field, \mathbf{J} is the electric current density, \mathbf{E} is the electric field, ρ , \mathbf{v} , p , and T are the plasma mass density, velocity, pressure, and temperature, $\mathbf{g} = -g_0 R_S^2 \hat{\mathbf{r}}/r^2$ is the gravitational acceleration, η the resistivity, and ν is the kinematic viscosity. Equation (10) contains the radiation loss function $Q(T)$, n_e and n_p are the electron and proton number density (which are equal for a hydrogen plasma), m_p is the proton mass, γ is the polytropic index, H_{ch} is the coronal heating term, and \mathbf{q} is the heat flux. The wave pressure term p_w in equation (9) represents the contribution due to Alfvén waves and is evolved using the WKB approximation for time-space averaged Alfvén wave energy density ϵ [Mikić

et al., 1999]. The method of solution of equation (6) through (9), including the boundary conditions, has been described previously [Mikić and Linker, 1994; Linker and Mikić, 1997; Lionello *et al.*, 1999; Mikić *et al.*, 1999; Linker *et al.*, 2001; Lionello *et al.*, 2009]. In the work presented here, however, we simplify these equations by employing a “polytropic” energy equation, where $S = 0$ [Usmanov, 1993; Mikić *et al.*, 1996; Usmanov, 1996; Linker *et al.*, 1999; Mikić *et al.*, 1999; Riley *et al.*, 2001a, 2002, 2003; Roussev *et al.*, 2003] and employ an empirical technique for deriving the speed profile for the inner boundary of the heliospheric model. Although such an approximation is at odds with observations (it requires that we set $\gamma = 1.05$ in the coronal model, for example), we have found that this approach for deriving solar wind speed is, at least currently, more accurate than can be obtained from the more self-consistent thermodynamic approach (P. Riley *et al.*, A multi-observatory inter-calibration of line-of-sight diachronic solar magnetograms and implications for the open flux of the heliosphere, submitted to *Astrophysical Journal*, 2010).

[17] Figure 6 compares model results with STEREO and ACE observations for CR 2060, which occurred during one of the intervals identified as “lulls.” The solid lines show model solutions, which were extracted by flying the spacecraft trajectories through the simulation domain. We note that the relative phasing of the streams at the three locations is captured in the model results. The fast stream centered on day 240, for example, is first seen at STEREO B, then ACE, and finally at STEREO A. Moreover, the general large-scale stream structure for this rotation is reproduced by the model: Generally slow and variable wind during the first half, followed by a large stream at day 240, and two smaller streams following it. The precise phasing of the modeled streams relative to the observations does not match up well, however: The first stream is predicted to arrive earlier than it actually does and the second stream is predicted to arrive later. Overall, however, these relatively typical results match sufficiently well that the model can be used to interpret the observations. The bottom summarizes the polarity of the radial component of the magnetic field. Both model and observations suggest an essentially two-sector pattern for this rotation.

[18] Figure 7 summarizes the computed coronal hole boundaries for CRs 2058 through 2063. These maps mark regions of open field lines (dark grey) and closed field lines (light grey) at the photosphere. We note that, during this time, there were well-defined polar coronal holes, together with equatorward extensions to these holes, as well as low and midlatitude holes, not obviously connected to other open field regions. The quantitative steps taken to compute the speed profiles in the model are described by Riley *et al.* [2001a]. In brief, a velocity profile at the photosphere, consisting of fast wind everywhere with slow wind localized at the boundaries between the open and closed field lines, is mapped outward along the field lines to $30 R_S$. Figure 8 shows the results of that mapping. Specifically, it shows the bulk radial solar wind velocity at $30 R_S$ for each of these six rotations. The trajectories of ACE, STEREO A, and STEREO B are overlaid. Since Carrington longitude increases from left to right in each frame, time proceeds from right to left. Thus, with increasing time, the spacecraft sample progressively earlier Carrington longitudes.

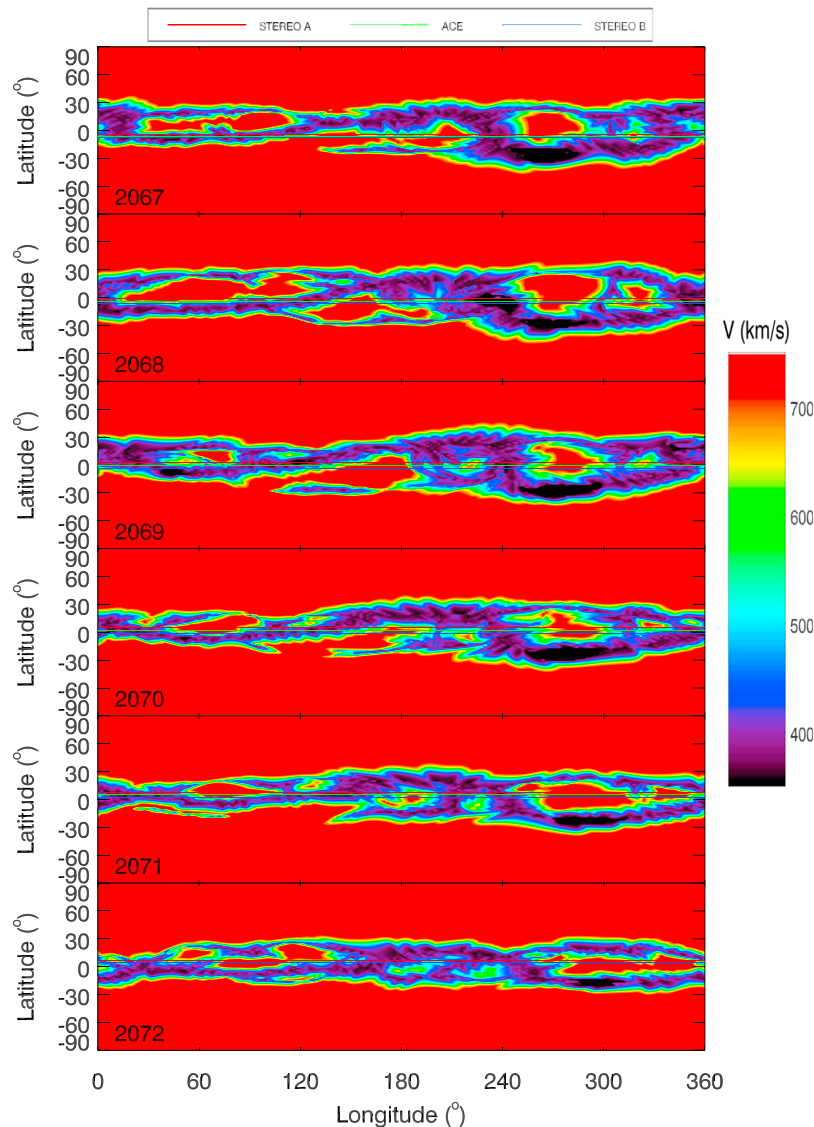


Figure 10. As in Figure 8, but for CRs 2067 through 2072.

[19] The connection between the computed coronal holes in Figure 7 and the high-speed streams within Figure 8 can, at least qualitatively, be understood; however, it is clear that the topology of the field lines between $1 R_S$ and $30 R_S$ has added a great deal of complexity to the velocity map. From Figure 8, we note the following points. First, the spacecraft were essentially located at the same heliographic latitude during this interval. Certainly, based on the quality of the match shown in Figure 6, we could not reliably ascribe any spatial inhomogeneities to these modest separations. Second, the three high-speed streams intercepted by all three spacecraft, initially at $\sim 120^\circ$ in CR 2059 and $\sim 210^\circ$ and $\sim 340^\circ$ in CR 2060 drift westward in the ensuing rotations.

[20] Figures 9 and 10 show coronal hole boundaries and speed profiles for CRs 2067 through 2072, which span the second “lull.” For this interval, we note the following. First, the spacecraft were separated more substantially in heliographic latitude. Second, again, there was a westward progression of the high-speed streams that were intercepted by

the spacecraft. Third, the stream boundaries tended to have a systematic tilt to them. This can be seen more clearly in the low-latitude coronal holes, which are orientated from SE to NW. The fast streams have a more complex profile, however, there is a tendency for STEREO A, which is at the highest heliographic latitude, to intercept the matching stream interface at a more westerly longitude.

5. Interpretation

[21] There are two obvious ways that the linear relationship between time lag and the increasing longitude of the ACE and STEREO spacecraft can be broken: temporal changes and/or spatial inhomogeneities. In the case of the latter, the pattern at the Sun does not change in time so that the structure of the solar wind in a frame rotating with the Sun is stationary; that is, it is strictly corotating. However, if the spacecraft are not located at exactly the same heliographic latitude, they will intercept different plasma sources. Consider, for example, an

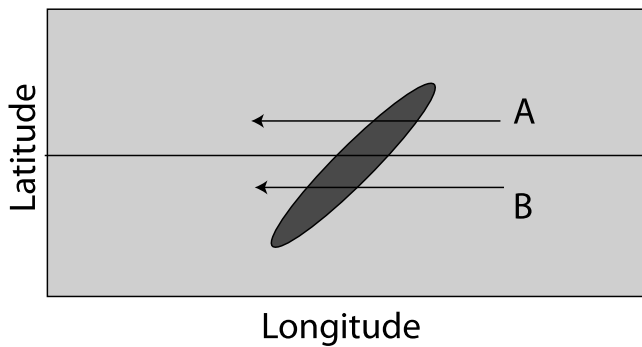


Figure 11. Schematic illustration of how the orientation of a coronal hole can affect the phase lag between two spacecraft, i.e., STEREO A and B. Their trajectory through the coronal hole are marked by horizontal arrows.

idealized, elongated low-latitude coronal hole, oriented so that one end is in the SE and the other end lies in the NW. This is shown schematically in Figure 11. If STEREO A is located at a higher heliographic latitude than either ACE or STEREO B, then the CH, and hence fast solar wind stream, will arrive slightly earlier than predicted since it is rooted in a more western source. Temporal effects can be understood in a similar way. If a low-latitude CH evolves in time so that it shifts toward the west as the structure passes from STEREO B to ACE and onto STEREO A, then the stream will arrive earlier than predicted by equation (3). Both of these examples, thus, lead to the “lulls” we have identified in the data. Clearly, in principle, it is possible for the opposite effects to take place: Structure that is oriented from the NE to SW or temporal evolution of structure that tends to precess in the Carrington frame would drive larger time lags. Our model results, however, do not provide any examples of this occurring during the STEREO timeframe. Instead, surrounding CR 2061, the general trend was for structures intercepted by the spacecraft to drift westward, while surrounding CR 2070,

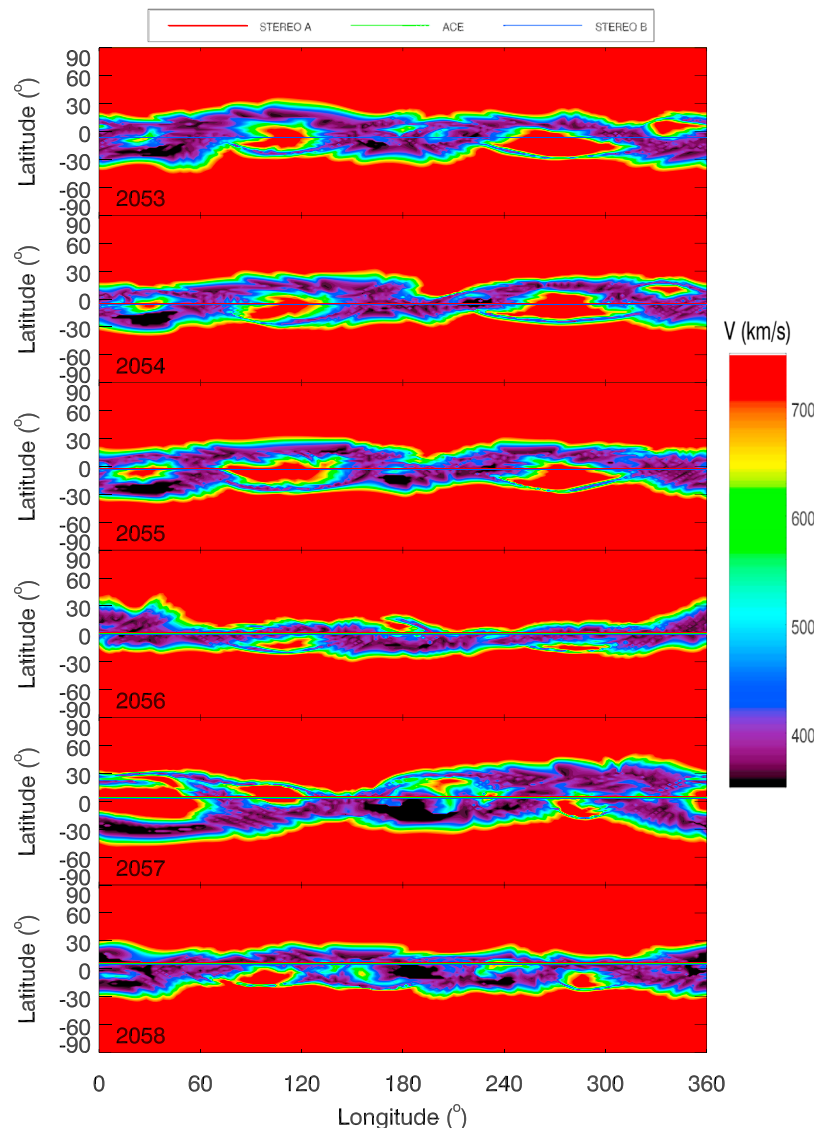


Figure 12. As in Figure 8, but for CRs 2053 through 2058.

both spatial and temporal effects likely contributed to the “lulls.” In particular, the stream interfaces were oriented from the SE to NW, so that wind from the same coronal hole arrived earlier than would have been predicted, and the coronal hole structure evolved such that the fast wind streams migrated westward. The variations in the peak cross-correlation coefficient during these lulls also provide some clues as to the nature of the processes producing them. In all three cases, the peak coefficient was as large, or slightly larger than surrounding values during the first lull, but was markedly lower during the second lull. This suggests a more transient, or nonsteady component to the processes producing the second lull.

[22] As a final verification of this interpretation, we consider the first 6 Carrington rotations of the STEREO mission. During this interval, the phase lag of the signals at all three spacecraft matched the linear increase predicted by equation (3). The computed solar wind velocities at $30 R_S$ for this interval are shown in Figure 12. During CR 2053 through 2055 the CCFs were driven by a stable pattern involving two long-lived equatorial coronal holes (at longitudes of $\sim 110^\circ$ and $\sim 270^\circ$). The spacecraft were not significantly separated in latitude, and thus, we would not expect spatial inhomogeneities to drive a deviation in the time lag. Moreover, there was no systematic evolution of the coronal holes during this interval. On the basis of these results, then, we would not expect any deviations in the time lag profile. During the second half of this interval, the wind sampled by the spacecraft was slow, variable, and unorganized. Again, there were no obvious systematic trends.

[23] Finally, it is worth noting that our analysis has tacitly assumed a fixed rotation period of 27.27 days. However, due to the super-radial expansion of the solar magnetic field, the plasma may originate from a range of heliographic latitudes. Lee *et al.* [2008] have shown that long-lived, high-speed streams may recur with periodicities in the range of 26.5–27.3 days. Using the Snodgrass formula for differential rotation of the photosphere [Snodgrass, 1983], this would suggest a source latitude lower than 43.4° , which $\tau_{rot} = 27.3$ days would imply. Although the sense of this effect is in the same direction as the lulls we have identified, its magnitude is too small to explain them: The lulls suggest deviations of >30 h away from 27.27 days, whereas the effects described by Lee *et al.* [2008] were limited to a fraction of a day. Nevertheless, this effect may contribute to some of the smaller deviations evident in Figures 3–5.

6. Summary

[24] In this study, we have applied a cross-correlation analysis to ACE, STEREO A, and B bulk solar wind velocity measurements for the period from STEREO’s launch through mid-2009. We found that, as with previous studies [Podesta *et al.*, 2008; Opitz *et al.*, 2009], there is a general trend for the phase lag between the streams to increase within increasing separation of the spacecraft. We also identified two intervals that deviated significantly from this trend. The first, centered around CR 2060, was previously identified by Opitz *et al.* [2009]. We used global MHD simulation results to understand these “lulls” in terms of both temporal evolution of the streams, as they swept first past STEREO B, then ACE, and finally past STEREO A, as well as spatial inhomogene-

ities, such that the spacecraft, separated in latitude by up to $\sim 14^\circ$ sampled different portions of the streams. Finally, beyond a separation of $\sim 77/36/30^\circ$, between STEREO A-B/STEREO A-ACE/ACE-STEREO-B, corresponding to an interval of approximately ~ 1.6 years, the CCF peaked at values <0.5 , suggesting that from this point, correlation analysis must be applied and interpreted with considerably more caution.

[25] **Acknowledgments.** PR, ZM, and JAL gratefully acknowledge the support of the LWS Strategic Capabilities Program (NASA, NSF, and AFOSR), the NSF Center for Integrated Space Weather Modeling (CISM), NASA’s Heliophysics Theory Program (HTP), and the NASA STEREO IMPACT and SECCHI teams. We thank the SWEPAM/ACE and PLASTIC/STEREO teams for providing data.

References

- Detman, T. R., M. Dryer, T. Yeh, S. M. Han, and S. T. Wu (1991), A time-dependent, three-dimensional MHD numerical study of interplanetary magnetic draping around plasmoids in the solar wind, *J. Geophys. Res.*, *96*(A6), 9531–9540, doi:10.1029/91JA00443.
- Dryer, M., Z. K. Smith, E. J. Smith, J. D. Mihalov, J. H. Wolfe, R. S. Steinolfson, and S. T. Wu (1978), Dynamic MHD modeling of solar wind corotating stream interaction regions observed by Pioneer 10 and 11, *J. Geophys. Res.*, *83*(A9), 4347–4352, doi:10.1029/JA083iA09p04347.
- Endler, F. (1971), Wechselwirkung zwischen Sonnenwind und koronalen Magnetfeldern, *Mitteilungen Astron. Gesellschaft Hamburg*, *30*, 136.
- Galvin, A. B., et al. (2008), The Plasma and Suprathermal Ion Composition (PLASTIC) investigation on the STEREO observatories, *Space Sci. Rev.*, *136*, 437–486, doi:10.1007/s11214-007-9296-x.
- Gosling, J. T., and S. J. Bame (1972), Solar-wind speed variations 1964–1967: An autocorrelation analysis, *J. Geophys. Res.*, *77*(1), 12–26, doi:10.1029/JA077i001p00012.
- Gosling, J. T., J. R. Asbridge, S. J. Bame, and W. C. Feldman (1976), Solar wind speed variations: 1962–1974, *J. Geophys. Res.*, *81*(28), 5061–5070, doi:10.1029/JA081i028p05061.
- Lee, C. O., et al. (2008), Manifestations of solar differential rotation in the solar wind: An update, *Eos Trans. AGU*, *89*, Spring Meet. Suppl., Abstract SH31A-02.
- Linker, J. A., and Z. Mikić (1997), Extending coronal models to earth orbit, in *Coronal Mass Ejections*, edited by N. Crooker, J. Joselyn, and J. Feynmann, p. 269, AGU, Washington, D. C.
- Linker, J. A., G. van Hoven, and D. D. Schnack (1990), A three-dimensional simulation of a coronal streamer, *Geophys. Res. Lett.*, *17*(13), 2281–2284, doi:10.1029/GL017i013p02281.
- Linker, J. A., et al. (1999), Magnetohydrodynamic modeling of the solar corona during whole Sun month, *J. Geophys. Res.*, *104*(A5), 9809–9830, doi:10.1029/1998JA900159.
- Linker, J. A., R. Lionello, Z. Mikić, and T. Amari (2001), Magnetohydrodynamic modeling of prominence formation within a helmet streamer, *J. Geophys. Res.*, *106*(A11), 25,165–25,175, doi:10.1029/2000JA004020.
- Lionello, R., Z. Mikić, and J. A. Linker (1999), Stability of algorithms for waves with large flows, *J. Comput. Phys.*, *152*(1), 346–358.
- Lionello, R., J. A. Linker, and Z. Mikić (2001), Including the transition region in models of the large-scale solar corona, *Astrophys. J.*, *546*(1), 542–551.
- Lionello, R., J. A. Linker, and Z. Mikić (2009), Multispectral emission of the sun during the first whole Sun month: Magnetohydrodynamic simulations, *Astrophys. J.*, *690*, 902–912, doi:10.1088/0004-637X/690/1/902.
- Manchester, W. B., A. J. Ridley, T. I. Gombosi, and D. L. Dezeewu (2006), Modeling the Sun-to-Earth propagation of a very fast CME, *Adv. Space Res.*, *38*, 253–262, doi:10.1016/j.asr.2005.09.044.
- McComas, D. J., S. J. Bame, P. Barker, W. C. Feldman, J. L. Phillips, P. Riley, and J. W. Griffée (1998), Solar wind electron proton alpha monitor (swepam) for the advanced composition explorer, *Space Sci. Rev.*, *86*(1–4), 563–612.
- Mikić, Z., and J. A. Linker (1994), Disruption of coronal magnetic field arcades, *Astrophys. J.*, *430*, 898–912.
- Mikić, Z., J. A. Linker, and J. A. Colborn (1996), An MHD Model of the solar corona and solar wind, *BAAS*, *28*, 868.
- Mikić, Z., J. A. Linker, D. D. Schnack, R. Lionello, and A. Tarditi (1999), Magnetohydrodynamic modeling of the global solar corona, *Phys. Plasmas*, *6*(5), 2217–2224.

- Mikić, Z., J. A. Linker, R. Lionello, and P. Riley (2002), Predicting the structure of the solar corona during the December 4, 2002 total solar eclipse, *Eos Trans AGU*, 83(47), Fall Meet. Abstract SH52A-0468.
- Mikić, Z., J. A. Linker, R. Lionello, P. Riley, and V. Titov (2007), Predicting the structure of the solar corona for the total solar eclipse of March 29, 2006, in *Solar and Stellar Physics Through Eclipses*, *Astron. Soc. Pac. Conf. Ser.*, vol. 370, edited by O. Demircan, S. O. Selam, and B. Albayrak, pp. 299, Side, Turkey.
- Odstrcil, D. (1994), Interactions of solar wind streams and related small structures, *J. Geophys. Res.*, 99(A9), 17,653–17,671, doi:10.1029/94JA01225.
- Odstrcil, D., J. A. Linker, R. Lionello, Z. Mikić, P. Riley, V. J. Pizzo, and J. G. Luhmann (2002), Merging of coronal and heliospheric numerical 2-d mhd models, *J. Geophys. Res.*, 107(A12), 1493, doi:10.1029/2002JA009334.
- Odstrcil, D., V. J. Pizzo, J. A. Linker, P. Riley, R. Lionello, and Z. Mikić (2004), Initial coupling of coronal and heliospheric numerical magnetohydrodynamic codes, *J. Atmos. Sol. -Terr. Phys.*, 66, 1311–1320.
- Opitz, A., et al. (2009), Temporal evolution of the solar wind bulk velocity at solar minimum by correlating the STEREO A and B PLASTIC measurements, *Sol. Phys.*, 256, 365–377, doi:10.1007/s11207-008-9304-7.
- Paularena, K. I., G. N. Zastenker, A. J. Lazarus, and P. A. Dalin (1998), Solar wind plasma correlations between IMP 8, INTERBALL-1, and WIND, *J. Geophys. Res.*, 103(A7), 14,601–14,618, doi:10.1029/98JA00660.
- Pizzo, V. (1978), A three-dimensional model of corotating streams in the solar wind: I. Theoretical foundations, *J. Geophys. Res.*, 83(A12), 5563–5572, doi:10.1029/JA083iA12p05563.
- Pneuman, G. W., and R. A. Kopp (1971), Gas-magnetic field interactions in the solar corona, *Sol. Phys.*, 18, 258–270.
- Podesta, J. J., A. B. Galvin, and C. J. Farrugia (2008), Correlation length of large-scale solar wind velocity fluctuations measured tangent to the Earth's orbit: First results from Stereo, *J. Geophys. Res.*, 113, A09104, doi:10.1029/2007JA012865.
- Richardson, J. D., F. Dashevskiy, and K. I. Paularena (1998), Solar wind plasma correlations between L1 and Earth, *J. Geophys. Res.*, 103(A7), 14,619–14,630, doi:10.1029/98JA00675.
- Riley, P. (2007), Modeling corotating interaction regions: From the Sun to 1 AU, *J. Atmos. Sol. -Terr. Phys.*, 69, 32–42, doi:10.1016/j.jastp.2006.06.008.
- Riley, P., J. T. Gosling, L. A. Weiss, and V. J. Pizzo (1996), The tilts of corotating interaction regions at midheliographic latitudes, *J. Geophys. Res.*, 101(A11), 24,349–24,357, doi:10.1029/96JA02447.
- Riley, P., J. A. Linker, and Z. Mikić (2001a), An empirically driven global MHD model of the corona and inner heliosphere, *J. Geophys. Res.*, 106(A8), 15,889–15,901, doi:10.1029/2000JA000121.
- Riley, P., J. A. Linker, Z. Mikić, and R. Lionello (2001b), Mhd modeling of the solar corona and inner heliosphere: Comparison with observations, in *Space Weather, Geophys. Monogr. Ser.*, vol. 125, edited by P. Song, H. J. Singer, and G. L. Siscoe, p. 159, AGU, Washington, D. C.
- Riley, P., J. A. Linker, and Z. Mikić (2002), Modeling the heliospheric current sheet: Solar cycle variations, *J. Geophys. Res.*, 107(A7), 1136, doi:10.1029/2001JA000299.
- Riley, P., Z. Mikić, and J. A. Linker (2003), Dynamical evolution of the inner heliosphere approaching solar activity maximum: Interpreting ulysses observations using a global mhd model, *Ann. Geophys.*, 21(6), 1347–1357.
- Riley, P., R. Lionello, Z. Mikić, J. Linker, E. Clark, J. Lin, and Y.-K. Ko (2007), “Bursty” reconnection following solar eruptions: MHD simulations and comparison with observations, *Astrophys. J.*, 655, 591–597, doi:10.1086/509913.
- Rouillard, A. P., et al. (2009), A multispacecraft analysis of a small-scale transient entrained by solar wind streams, *Sol. Phys.*, 256, 307–326, doi:10.1007/s11207-009-9329-6.
- Roussev, I. I., T. I. Gombosi, I. V. Sokolov, M. Velli, W. Manchester, D. L. DeZeeuw, P. Liewer, G. Tóth, and J. Luhmann (2003), A three-dimensional model of the solar wind incorporating solar magnetogram observations, *Astrophys. J. Lett.*, 595(1), L57–L61.
- Smith, Z., and M. Dryer (1990), Mhd study of temporal and spatial evolution of simulated interplanetary shocks in the ecliptic-plane within 1 au, *Sol. Phys.*, 129, 387–405.
- Snodgrass, H. B. (1983), Magnetic rotation of the solar photosphere, *Astrophys. J.*, 270, 288–299, doi:10.1086/161121.
- Steinolfson, R. S., S. T. Suess, and S. T. Wu (1982), The steady global corona, *Astrophys. J.*, 255, 730–742, doi:10.1086/159872.
- Stone, E. C., A. M. Frandsen, R. A. Mewaldt, E. R. Christian, D. Margolies, J. F. Ormes, and F. Snow (1998), The advanced composition explorer, *Space Sci. Rev.*, 86, 1–22, doi:10.1023/A:1005082526237.
- Usmanov, A. V. (1993), A global numerical 3-D MHD model of the solar wind, *Sol. Phys.*, 146, 377–396, doi:10.1007/BF00662021.
- Usmanov, A. V. (1996), A global 3-d mhd solar wind model with Alfvén waves, *Int. Solar Wind Conf.*, 382, 141–144.

J. A. Linker, Z. Mikić, and P. Riley, Predictive Science, San Diego, CA 92121, USA.

J. Luhmann, SSL, University of California, Berkeley, CA 94720, USA.

A. Opitz, Centre d'Etude Spatiale des Rayonnements (CNRS-UPS), University of Toulouse, F- 31028 Toulouse, France.